Optik - International Journal for Light and Electron Optics 192 (2019) 162933

Contents lists available at ScienceDirect

Optik

journal homepage: www.elsevier.com/locate/ijleo

Study of satellite imaging with pitch motion compensation to increase SNR

Tingting Xu[a,b], Xiubin Yang[a,c,*], Chao Xu[a,b], Lin Chang[a,c], Lin Zhu[a,b]

[a] Changchun Institute of Optics, Fine Mechanics and Physics, Changchun, 130033, China
[b] University of Chinese Academy of Sciences, Beijing, 100049, China
[c] National & Local United Engineering Research Center of Small Satellite Technology, Changchun, 130033, China

ARTICLE INFO

Keywords:
Pitch motion compensation
Hyperspectral camera
Signal to noise ratio (SNR)
Integral time
Remote sensing
ZH-1

ABSTRACT

Aiming at the short integral time and low signal-to-noise ratio(SNR) of the large field hyperspectral camera push-broom imaging, a new imaging mode of satellite with pitch motion compensation is proposed to increase the integral time, so that the SNR of the instrument can be improved. Firstly, the relationship between integral time and SNR is derived, and then the pitch angular velocity is calculated and utilized to make the satellite scan in a maneuverable manner. Finally, the on-orbit pitch motion compensation imaging test is carried out by ZH-1, and the remote sensing images with higher SNR than the conventional push-broom images are obtained, which validate the theory. The imaging mode proposed in this paper can not only improve the SNR without changing the inherent optical parameters of the camera, but also reduce the cost of hyperspectral camera and expand the scope of application.

1. Introduction

Hyperspectral remote sensing imaging technology is a combination of imaging and spectral technology, which can obtain the image information and continuous spectrum information of the target at the same time, has been deeply applied to land, ocean, aerosol and other fields. [1] With the rapid development of devices such as photodetectors and spectrophotometry elements, the spatial resolution, spectral resolution and detection sensitivity are becoming higher [2]. We hope that hyperspectral remote sensing system can achieve compact structure, low cost, simple installation and modular production. However, for the existing interferometric and dispersive hyperspectral imaging systems, in order to obtain a higher spectral resolution, the width of the incident slit should be reduced. As a result, the radiance received by the detector will be greatly reduced, which directly affects the SNR and seriously reduces the image quality [3–6].

In order to ensure that the SNR of remote sensing images is high enough, a series of techniques to improve SNR are proposed by researchers. One approach is to use scanning mirror with motion compensation to increase the integral time, which is applied to High Resolution Imaging Spectrometer (HIRIS) [7], Costal Ocean Imaging Spectrometer(COIS) [8]. However, the scanning mirror institution, including precision stepping motor, large speed ratio reducer and position sensor, has a high complexity of system structure, high requirements on hardware, as well as quality and volume constraints on the load platform. Another kind of approach is to improve the optical system, such as Large Aperture Static Imaging Spectrometer(LASIS) proposed by Xi ' an Institute of Optics and Precision Mechanics. There are no moving parts or slits used to limit the Field of View(FOV) in LASIS, and the high input radiation and SNR can be achieved, but the measurement of the spectrum of the system is non-real-time and high performance detectors are

* Corresponding author at: Changchun Institute of Optics, Fine Mechanics and Physics, Changchun, 130033, China.
E-mail address: yangxiubin@ciomp.ac.cn (X. Yang).

https://doi.org/10.1016/j.ijleo.2019.162933
Received 23 March 2019; Accepted 11 June 2019

required.

The satellite ZH-1 mentioned in this paper is a hyperspectral microsatellite with compact structure, small size and light weight, the spectral imaging system is based on filter. The technologies mentioned above to improve the SNR of the system have heavy requirements for the detector and structural complexity, and cannot be applied to ZH-1. Therefore, when the optical parameters and detector of the system are determined, this paper proposes an imaging mode of satellite with pitch motion compensation, which can improve the SNR of the system without changing the internal parameters of the optical system. The following part firstly deduces the SNR expression from the theoretical model, and then the model of satellite pitch angular velocity is established and the relationship between integral time and SNR is analyzed.

2. Satellite pitch motion compensation imaging and signal-to-noise-ratio (SNR) model

The pitch motion compensation of hyperspectral satellite is based on the conventional push-broom imaging of the satellite, which can reduce the satellite pushing-broom velocity and increase the integral time. Once the parameters of the camera optical system are determined, the integral time can be adjusted to improve the imaging SNR.

2.1. Calculation of signal-to-noise-ratio (SNR)

SNR is an important technical index to evaluate the imaging quality of hyperspectral cameras, and the SNR equation of optical remote sensing imaging is as follows

$$SNR = \frac{N_s}{N_{noise}} \tag{1}$$

where N_s is the number of signal photons received by the camera during the integral time of the TDI detector and N_{noise} is the number of noise photons received at the same time. According to the specific parameters, the SNR expression with dB is

$$SNR = 20\lg\frac{\frac{\pi\eta M \cdot T_i\rho\tau_0 E_0\cos z}{4F^2(hc/\lambda)}}{\sqrt{\frac{\pi\eta M \cdot T_i\rho\tau_0 E_0\cos z}{4F^2(hc/\lambda)} + N_d + N_b}}(dB) \tag{2}$$

where η is the spectral quantum efficiency of the detector; hc/λ is the energy of a single photon; M is the integral series of TDI detector; T_i is the row shift time of the TDI detector; F is the reciprocal of the relative aperture of the optical system; ρ is the albedo; τ_0 is the system transmittance; z is the solar altitude angle; E_0 is the solar irradiance to the target, which can be calculated by MODTRAN [9]. Detector noise includes shot noise, dark current noise and output noise [10].

From Eq. (2), it can be seen that the integral time of the detector is proportional to the SNR. In other words, higher SNR can be achieved by increasing the integral time of imaging without changing the optical system and detector parameters. Therefore, in this paper, the method of satellite pitch maneuvering to compensate the imaging speed of push-broom along-track is used to adjust the integral time of TDI detector to increase the SNR of the camera.

2.2. Hyperspectral satellite pitch motion compensation imaging

The pitch motion compensation of hyperspectral satellite is based on the satellite maneuvering ability, which enables the satellite to pitch in the direction of the inverse push-broom imaging while flying, reduces the relative push-broom speed of the TDI camera and the ground, and increases the integral time of the TDI detector. The principle of satellite pitch motion compensation imaging is shown in Fig. 1. First, the attitude of the satellite is controlled to keep the direction of TDI imaging push-broom consistent with the direction of imaging trajectory. Then the satellite is made to rotate by a certain angle θ at the moment t_0 and pitch until the moment t_2 to complete a motion compensation. The distance from the nadir corresponding to the movement of the satellite from time t_0 to time t_2

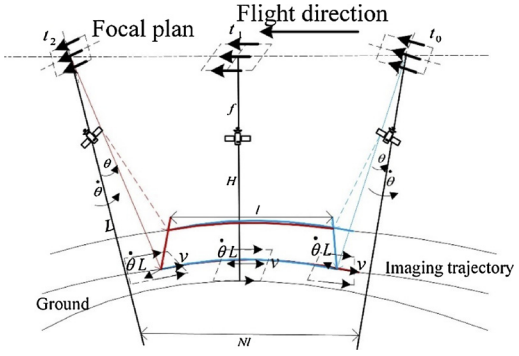

Fig. 1. Diagram of hyperspectral satellite pitch motion compensation imaging.

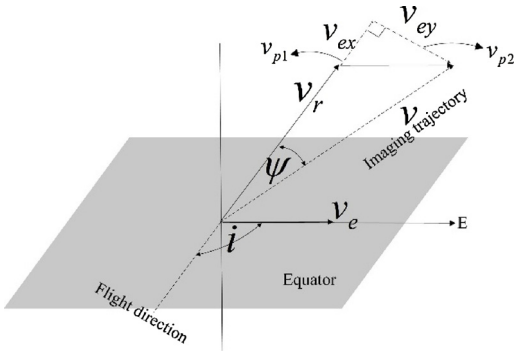

Fig. 2. Diagram of hyperspectral push-broom imaging resultant velocity.

is Nl, and the corresponding ground observation distance is l.Therefore, the integral time of the detector is N times that of the conventional push-broom imaging with no compensation. f is the focal length of the space camera, H is the orbital altitude, θ is the pitch angle, $\dot{\theta}$ is the pitch angular velocity, and L is the real-time distance between the satellite and the ground object target.

2.2.1. Calculation of trajectory direction of hyperspectral satellite pitch motion compensation imaging

The pitch motion compensation imaging of hyperspectral satellites needs to make the direction of push-broom imaging consistent with the imaging trajectory. In the process of push-broom imaging, the target point T has not only the relative ground speed of the satellite v_r, but also the earth rotation speed v_e. Therefore, the actual imaging trajectory of the target point will deviate from the satellite flight direction by a certain angle, which can be represented by the yaw angle ψ. By calculating the resultant velocity v of the target point on the object surface, and then adjusting the yaw angle ψ of the satellite according to the vector direction by utilizing the maneuvering ability of the satellite, the push-broom direction can be consistent with the imaging trajectory. The velocity relation of the target point is shown in Fig. 2.

The resultant velocity vector v is composed of v_{p1} and v_{p2}, which represent the target's velocity along and across the satellite flight direction, respectively. v_{p1} includes the relative ground velocity v_r of the satellite and the projected velocity v_{ex} of the earth rotation velocity v_e along the satellite flight direction; Obviously, v_{p2} is equal to the projected velocity v_{ey} of the earth rotation velocity v_e across the satellite flight direction. The velocity vectors are expressed as follows.

$$v_r = \frac{R_e}{R_e + H}\sqrt{\frac{\mu}{R_e + H}} \tag{3}$$

$$v_e = \omega_e R_e \cos\delta_t \tag{4}$$

$$v_{ex} = v_e \cos(\pi - i) \tag{5}$$

$$v_{ey} = v_e \sin(\pi - i) \tag{6}$$

$$v_{p1} = v_r + v_{ex} = v_r - \omega_e R_e \cos\delta_t \cos i \tag{7}$$

$$v_{p2} = v_{ey} = v_e \sin i \tag{8}$$

The combined velocity of the target deviating from the satellite flight direction can be expressed as yaw angle [11] ψ:

$$\psi = \arctan\frac{v_{p2}}{v_{p1}} = \arctan\frac{\omega_e R_e \cos\delta_t \sin i}{v_r - \omega_e R_e \cos\delta_t \cos i} \tag{9}$$

The yaw angle is adjusted so that the TDI push-broom direction can be consistent with the combined velocity direction. It can be seen from the above formulas that the yaw angle of the satellite is independent of the internal parameters of the hyperspectral camera, but it will decrease monotonously with the decrease of the latitude of the target point. R_e is the radius of the earth, H is the orbital altitude, μ is the gravitational constant of the earth, i is the orbital inclination of the satellite, ω_e is the angular velocity of the earth's rotation, and δ_t is the latitude of the target point.

2.2.2. Calculation of satellite pitch angular velocity

According to v_{p1} and v_{p2} calculated in section 2.2.1, the resultant velocity vector v at the target point is:

$$v = \sqrt{v_{p1}^2 + v_{p2}^2} = \sqrt{(v_r - v_e\cos i)^2 + (v_e \sin i)^2} \tag{10}$$

Since the satellite's pitching motion occurs in the flight direction, the imaging trajectory of the target point after pitching does not change, and it is still the direction of the resultant velocity. The velocity relation at the target point of the satellite pitch motion compensation imaging is shown in Fig. 3, where θ is the satellite pitch angular velocity, and v_p is the relative ground flight velocity of the satellite after motion compensation, which changes in real time with the adjustment of integral time. According to Fig. 3, the

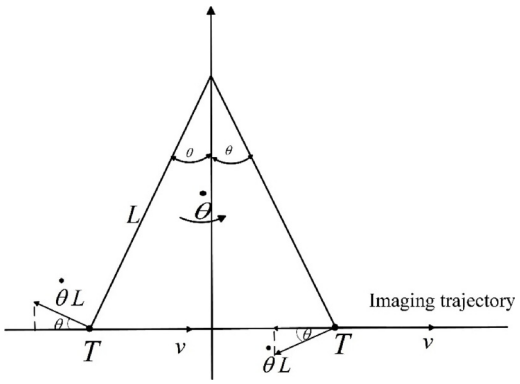

Fig. 3. Composite diagram of pitch motion compensation imaging velocity of hyperspectral satellite.

velocity relationships are as follows:

$$v_p = v - \dot{\theta} L \cos\theta \tag{11}$$

$$L = \frac{H}{\cos\theta} \tag{12}$$

All the above discussions are carried out on the object plane. According to the mapping relationship between the object plane and the image plane, it is easy to get the image motion velocity on the image plane as,

$$v_{image} = \frac{f}{H} v_p \tag{13}$$

Substitute Eq. (10) into Eq. (13) to get,

$$v_{image} = \frac{f\left(\sqrt{(v_r - v_e\cos i)^2 + (v_e \sin i)^2} - \dot{\theta} L \cos\theta\right)}{H} \tag{14}$$

When the integral time of the detector is increased by N times of that of the conventional push-broom imaging, the integral time can be expressed as follows:

$$NT_i = \frac{a}{v_{image}} = \frac{aH}{f\left(\sqrt{(v_r - v_e\cos i)^2 + (v_e \sin i)^2} - \dot{\theta} L \cos\theta\right)} \tag{15}$$

Thus, the satellite pitch angular velocity can be obtained as follows:

$$\dot{\theta} = \frac{a \times H \times \sqrt{(v_r - v_e\cos i)^2 + (v_e \sin i)^2} - N \times T_i \times f}{a \times H \times L \times \cos\theta} \tag{16}$$

By substituting Eq. (3) and Eq. (4) into Eq. (16), the satellite pitch angular velocity can be obtained as

$$\dot{\theta} = \frac{\sqrt{\left(\frac{R_e}{R_e+H}\sqrt{\frac{\mu}{R_e+H}} - \omega_e \times R_e \times \cos\delta_t \times \cos i\right)^2 + (\omega_e \times R_e \times \cos\delta_t \times \sin i)^2} - N \times T_i \times f}{H} \tag{17}$$

It can be known from Eq. (17) that when the satellite orbit parameters and the internal optical parameters of the hyperspectral camera remain unchanged, increasing the integral time will make the satellite attitude change in real time. This imaging method can improve the SNR without the need to change the internal optical parameters of the hyperspectral camera.

3. Terminal sliding mode control method

Terminal sliding mode control algorithm can image stably with the hyperspectral satellite attitude changes in real time. The algorithm changes the strategy of using linear sliding mode to control the traditional sliding mode variable structure and introduces the nonlinear function in the design of sliding hyperplane. According to the expected attitude deviation obtained by the planning, the system tracking error on the sliding surface can converge to zero in a limited time, so as to realize the accurate tracking of the expected imaging process. The satellite dynamics and kinematics equations are as follows [12]:

$$\dot{\rho} = \frac{1}{4}[(1 - \rho^T\rho)I_{3\times3} + 2\tilde{\rho} + 2\rho\rho^T]\omega = F(\rho)\omega = f_1(\rho, \omega)v \tag{18}$$

$$\dot{\omega} = -J^{-1}\omega \times (J\omega) + J^{-1}u + J^{-1}T_{ext} = f_2(\rho, \omega) + Bu + J^{-1}T_{ext} \tag{19}$$

Where ρ and ω represent the attitude angle and attitude angular velocity of the satellite, J represents the moment of inertia of the satellite, u is the calculated control moment, and T_{ext} is the external interference moment.

According to terminal sliding mode control method and Lyapunov stability theory [13], the control moment is as follows:

$$u = -b^{-1}[f - \ddot{\rho}_d - \ddot{p} + C_2^{-1}C_1(\dot{\rho}_e - \dot{p})] - b^{-1}\left(K\frac{C_2^T\sigma}{\| C_2^T\sigma \| + \delta_0 + \delta_1 \| \rho_e \|} + \frac{\partial f_1(\rho, \omega)}{\partial \omega}J^{-1}D\right) \tag{20}$$

and

$$f = \frac{\partial f_1(\rho, \omega)}{\partial \rho}f_1(\rho, \omega) + \frac{\partial f_1(\rho, \omega)}{\partial \omega}f_2(\rho, \omega),\ b = \frac{\partial f_1(\rho, \omega)}{\partial \omega}B$$

Where σ is the sliding mode surface function of the sliding mode control, which is a combination of the control deviation and parameters of the satellite, in the form of $\sigma = CE - W(t)$.

For the above satellite model, the specific decomposition form of the sliding mode surface function is as follows:

$$E = \begin{pmatrix}\rho_e \\ \dot{\rho}_e\end{pmatrix} = (\rho_{1e}, \rho_{2e}, \rho_{3e}, \dot{\rho}_{1e}, \dot{\rho}_{2e}, \dot{\rho}_{3e})^T,\ W(t) = CP(t),\ P(t) = \begin{pmatrix}p \\ \dot{p}\end{pmatrix}.\ C = (C_1, C_2)$$

$C_i = diag(c_{i1}, c_{i2}, c_{i3})$ is positive constant,

$$\begin{aligned} p(t) &= \rho_e(0) + \dot{\rho}_e(0)t + \frac{1}{2}\ddot{\rho}_e(0)t^2 \\ &+ \left[\frac{-10}{T^3}\rho_e(0) + \frac{-6}{T^2}\dot{\rho}_e(0) + \frac{-3}{2T}\ddot{\rho}_e(0)\right]t^3 \\ &+ \left[\frac{15}{T^4}\rho_e(0) + \frac{8}{T^3}\dot{\rho}_e(0) + \frac{3}{2T^2}\ddot{\rho}_e(0)\right]t^4 \\ &+ \left[\frac{-6}{T^5}\rho_e(0) + \frac{-3}{T^4}\dot{\rho}_e(0) + \frac{-1}{2T^3}\right]t^5 \end{aligned} \tag{21}$$

This method continues the general characteristics of the sliding mode control strategy, can reach the target attitude in a short time, and the system has stability and robustness. Through the above law of satellite attitude control, it is ensured that the control system has global asymptotic stability, and can effectively control the satellite to always track and point to the dynamic target, realize the agility maneuver of attitude and the stability of real-time tracking.

4. On-orbit imaging test of ZH-1

In order to evaluate the effectiveness of the SNR control algorithm of the satellite pitch motion compensation, an on-orbit imaging experiment was carried out using ZH-1.

4.1. Design of on-orbit imaging parameters of ZH-1

When the hyperspectral satellite is on orbit, the triaxial attitude of the satellite body coordinate system remains unchanged relative to the orbit coordinate system, and it is to carry out push-broom imaging along the flight direction. The imaging parameters of ZH-1 are shown in Table 1.

In the satellite pitch motion compensation imaging of ZH-1, the roll and pitch angle is stable in the zero-point attachment, and the corresponding roll and pitch angular velocity is also stable near the zero-point, yaw angle within 2.4° and 2.6° monotone increasing, the yaw angular velocity decreases monotonically with the decrease of the latitude of the imaging target with 0.003°/s. The integral time of the three TDI sensors in the focal plane of the push-broom imaging remained stable and decreased slightly with the change of latitude. During the 120 s imaging time, the latitude variation range of the imaging trajectory is 42°~50° (Figs. 4–7).

In the satellite pitch motion compensation imaging of the ZH-1, the roll angle is stable in the zero-point attachment, and the

Table 1
Imaging parameters on orbit.

Serial number	Imaging parameters on orbit	Value
1	Earth radius	6378km
2	Camera focal length	0.214m
3	Camera pixel size	4.25um
4	Orbit altitude	500km
5	Ground resolution	10m
6	Pitch angle	± 30°
7	Satellite velocity relative to the ground	7.43 km/s
8	Integral time of Nadir	1.4 ms
9	Swath width	150km

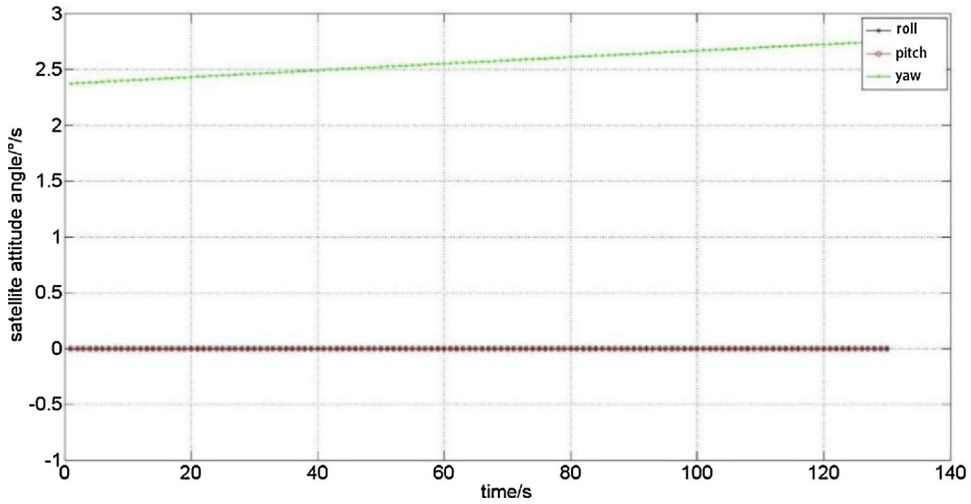

Fig. 4. The satellite attitude angle variation diagram of conventional push-broom imaging.

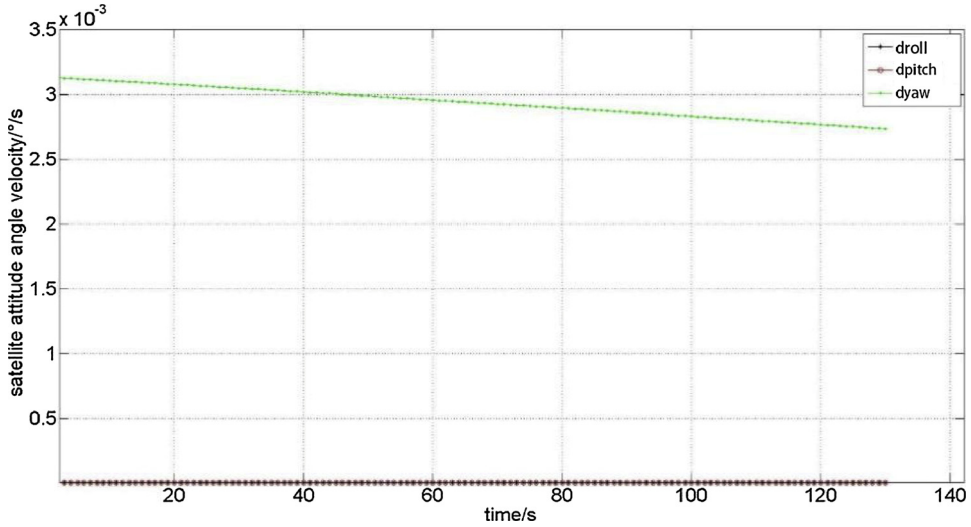

Fig. 5. The satellite attitude angular velocity variation diagram of conventional push-broom imaging.

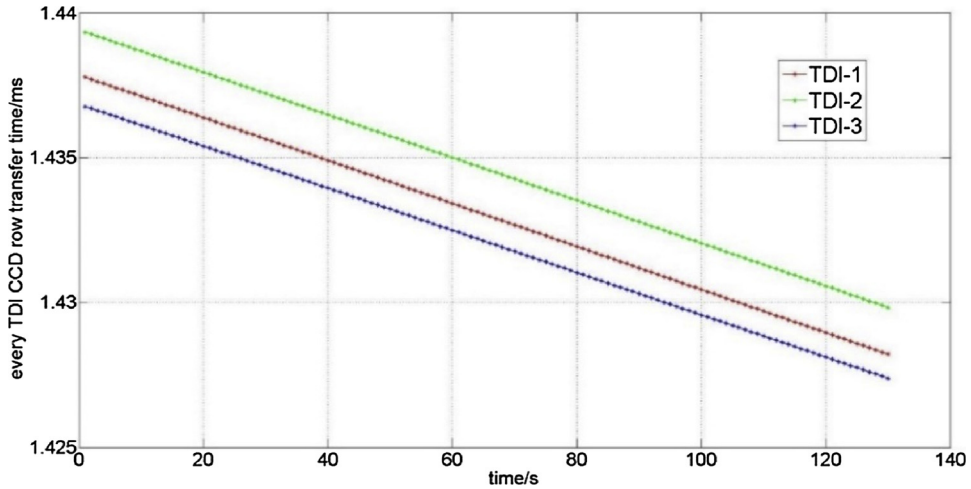

Fig. 6. Schematic of TDI integral time of conventional push-broom imaging with imaging time change.

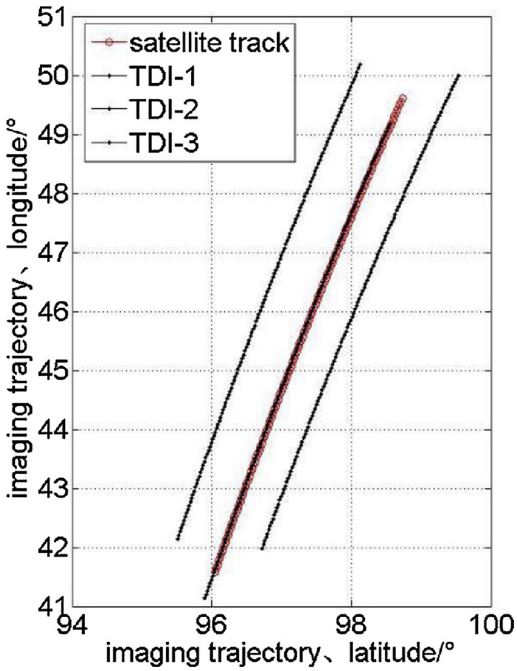

Fig. 7. Imaging trajectory of conventional push-broom imaging.

corresponding roll angular velocity is also stable near the zero-point. The pitch angle decreases from 20° to -25° within 120 s and the pitch angular velocity changes in parabolic form within the -0.2°/s˜-0.42°/s. The yaw angle within 2.4° and 2.6° monotone increasing and the yaw angular velocity decreases monotonically with the decrease of the latitude of the imaging target with 0.003°/s. The integral time of the second TDI detector in the focal plane of the pushing-broom imaging remained stable at 2.8 ms, while the other two pieces varied within 2.2ms˜4.5 ms due to the change of object distance. During the 120 s imaging time, the latitude variation range of the imaging trajectory is 43°˜48.5° (Figs. 8–11).

4.2. SNR analysis of ZH-1 satellite imaging

Eq. (2) shows that the SNR is affected by the detector's integral time, average quantum efficiency, integral series, pixel size, F number, the transmittance of the optical system, spectral bandwidth, solar altitude angle, surface reflectance and other parameters. Based on the design parameters of the ZH-1, the following part focuses on the numerical simulation analysis of the integral time of the detector.

Typical parameters are set as follows: TDI detector integral series $M = 2$, average quantum efficiency $\eta = 0.6$, detector pixel size is

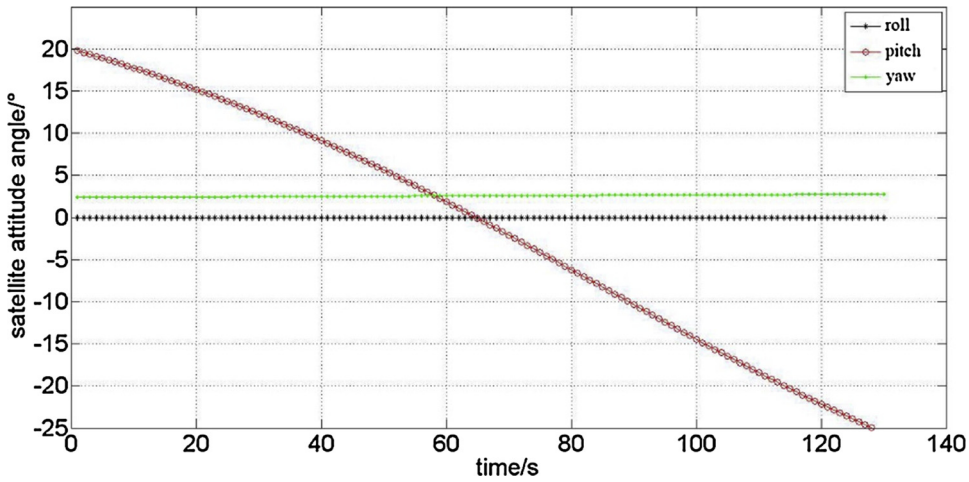

Fig. 8. The satellite attitude angle variation diagram of satellite pitch motion compensation imaging.

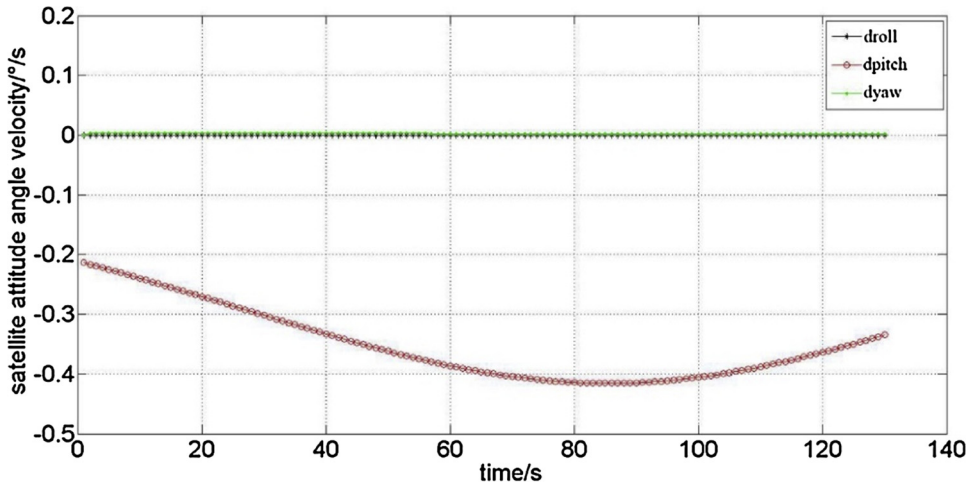

Fig. 9. The triaxial attitude angular velocity variation diagram of satellite pitch motion compensation imaging.

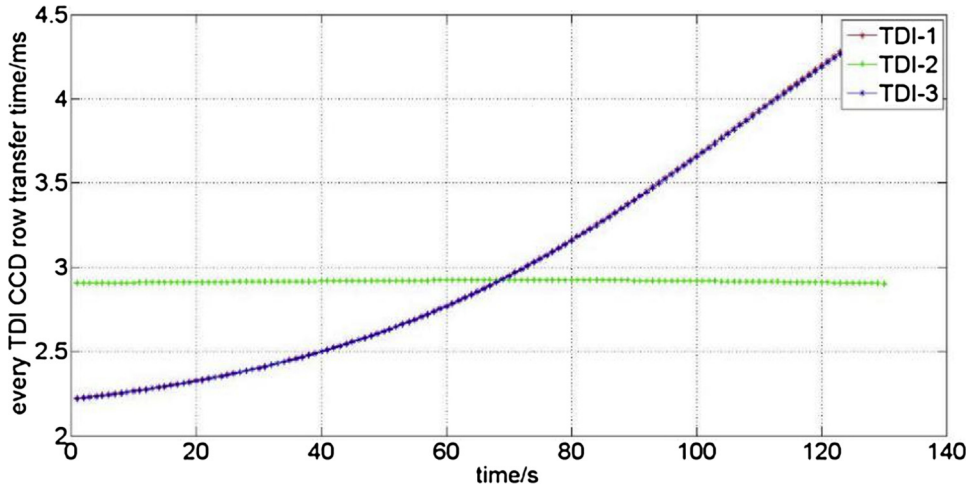

Fig. 10. Schematic of TDI integral time of satellite pitch motion compensation imaging.

4.25 μm, detector dark current noise and output noise can be ignored; Optical system transmittance $\tau_0 = 0.8$, F number is 4.5 and according to the optical system and detector parameters, the spectral bandwidth was selected as 3 nm, the spectral range is from 700 nm to 703 nm. Five solar altitude angles are chosen of 10°, 30°, 40°, 50°, 60°, and four kinds of surface reflectivity are used of 0.05, 0.20, 0.30, 0.65. The integral time was set as 1.4 ms. In the case of conventional push-broom imaging of hyperspectral satellite, the signal noise was calculated at 701 nm, as shown in Table 2.

When the integral time is adjusted to 2.8 ms to make the satellite with pitch motion compensation imaging, the signal noise is calculated at 701 nm, as shown in Table 3.

According to the data in Table 3 and Table 4, it can be intuitively seen that the SNR of different regions is improved after increasing the integral time, which confirms that the imaging mode proposed in this paper is correct and feasible in theory.

4.3. Analysis of ZH-1 on-orbit imaging

Fig. 12 shows the conventional on-orbit push-broom image of ZH-1 (integral time: 1.4 ms, SNR: about 30 dB). The image is a true color image synthesized by spectral segments of 688 nm, 538 nm and 486 nm. Fig. 13 shows the on-orbit pitch motion compensation (integral time: 2.8 ms, SNR: about 40 dB) image of the ZH-1. The image is a false-color image synthesized by spectral segments of 728 nm, 598 nm and 538 nm. It can be seen from the comparison of images using conventional push-broom imaging and pitch motion compensation imaging that increasing the integral time can effectively increase the SNR. However, due to the error factors such as image evaluation, the difference between ground features and spectral segments, there is a certain deviation in the SNR of on-orbit remote sensing images. This technique can be used as one of the ways to improve the SNR measurement of hyperspectral image.

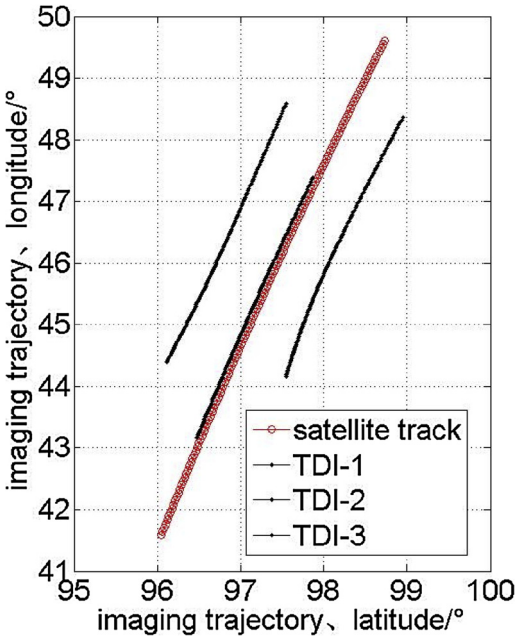

Fig. 11. Imaging trajectory satellite pitch motion compensation imaging.

Table 2
SNR of hyperspectral conventional push-broom imaging with an integral time of 1.4 ms.

Albedo	Solar altitude angle				
	10	30	40	50	60
0.05	21.1899	25.7829	26.8738	27.6357	28.1685
0.20	27.2105	31.8035	32.8944	33.6563	34.1891
0.30	28.9714	33.5644	34.6553	35.4172	35.9500
0.65	32.3293	36.9223	38.0133	38.7751	39.3079

Table 3
SNR of hyperspectral pitch motion compensation imaging with an integral time of 2.8 ms.

Albedo	Solar altitude angle				
	10	30	40	50	60
0.05	24.2002	28.7932	29.8841	30.6460	31.1788
0.20	30.2208	34.8138	35.9047	36.6666	37.1994
0.30	31.9817	36.5747	37.6656	38.4275	38.9603
0.65	35.3396	39.9326	41.0236	41.7854	42.3182

5. Conclusion

The satellite pitch motion compensation imaging mode proposed in this paper can improve the integral time without changing the inherent optical parameters of the camera. In addition, high SNR hyperspectral images were obtained using ZH-1, which verified the theory. It has played a positive role in reducing the cost and expanding the application range of hyperspectral cameras. In the future, we will further analyze the influence of the imaging mode on the SNR according to the constraint factors such as the performance of the detector and the selection of the imaging area, and try to reduce the influence of satellite attitude on the SNR in the process of maneuvering imaging by using the high stability satellite attitude control method.

Acknowledgments

This work is supported by National Natural Science Foundation of China [Grant No. 61705222].

Fig. 12. Conventional on-orbit push-broom images of ZH-1 (integral time 1.4 ms, SNR about 30 dB).

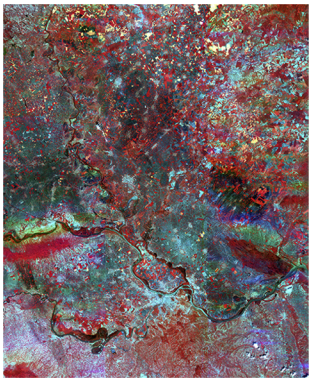

Fig. 13. Pitch motion compensation on-orbit images of ZH-1 (integral time: 2.8 ms, SNR: about 40 dB).

References

[1] C. Zhang, T. Mu, W. Ren, L. Zhang, N. Liu, Design and analysis of wide-field-of-view polarization imaging spectrometer, Opt. Eng. 49 (2010), https://doi.org/10.1117/1.3386079 258-258.

[2] J. Transon, R.D. Andrimont, A. Maugnard, P. Defourny, Survey of hyperspectral earth observation applications from space in the Sentinel-2 context, Remote Sens. 10 (2018) 157.

[3] M. Folkman, J. Pearlman, L. Liao, P. Jarecke, EO-1/Hyperion hyperspectral imager design, development, characterization, and calibration, in: W.L. Smith, Y. Yasuoka (Eds.), Hyperspectral Remote Sensing of the Land and Atmosphere, 2001, pp. 40–51.

[4] L. Jiang, X. Chen, G. Ni, D. Xu, H. Li, Hyperion true color images mosaic, in: L. Zhou, C.S. Li, M.M. Yeung (Eds.), Electronic Imaging and Multimedia Technology V, Pts 1 and 2, 2008 pp. Z8332-Z8332.

[5] I. Renhorn, D. Bergstrom, J. Hedborg, D. Letalick, S. Moller, High spatial resolution hyperspectral camera based on a linear variable filter, Opt. Eng. 55 (2016) 114105-114105.

[6] S. Yarbrough, T.R. Caudill, E.T. Kouba, V. Osweiler, J. Arnold, R. Quarles, J. Russell, L.J. Otten, B.A. Jones, A. Edwards, MightySat II.1 hyperspectral imager: summary of on-orbit performance, Proceedings of SPIE - The International Society for Optical Engineering, (2002), pp. 186–197.

[7] A.F.H. Goetz, M. Herring, The high-resolution imaging spectrometer (HIRIS) for EOS, IEEE Trans. Geosci. Remote. Sens. 27 (1989) 136–144, https://doi.org/10.1109/36.20291.

[8] C.O. Davis, Applications of hyperspectral imaging in the coastal ocean, in: S.S. Shen (Ed.), Imaging Spectrometry Viii, 2002, pp. 33–41.

[9] Y.H. Chen, Y.Q. Ji, J.K. Zhou, X.H. Chen, W.M. Shen, Optimization of the exposure time of aerospace camera through its signal-to-noise ratio, in: Y. Sheng, Y. Wang, L. Zeng (Eds.), International Conference on Optical Instruments and Technology: Optical Systems and Optoelectronic Instruments, Spie-Int Soc Optical Engineering (2008) 2009.

[10] J. Nieke, M. Solbrig, A. Neumann, Noise contributions for imaging spectrometers, Appl. Opt. 38 (1999) 5191–5194, https://doi.org/10.1364/ao.38.005191.

[11] B. Du, S. Li, Y. She, W. Li, H. Liao, H. Wang, Area targets observation mission planning of agile satellite considering the drift angle constraint, J. Astron. Telesc. Instrum. Syst. 4 (2018), https://doi.org/10.1117/1.Jatis.4.4.047002.

[12] S.C. Lo, Y.P. Chen, Smooth sliding-mode control for spacecraft attitude tracking maneuvers, J. Guid. Control. Dyn. 18 (1995) 1345–1349, https://doi.org/10.2514/3.21551.

[13] M.S. Branicky, Multiple Lyapunov functions and other analysis tools for switched and hybrid systems, IEEE Trans. Automat. Contr. 43 (1998) 475–482, https://doi.org/10.1109/9.664150.